





## Article

# Water CO<sub>2</sub> Emission Monitoring in a Romanian Peri-Urban Wetland to Enhance GHG Reporting

György Deák <sup>1,2</sup> , Natalia Enache <sup>1,2,\*</sup> , Lucian Laslo <sup>1</sup> , Monica Matei <sup>1</sup>, Madalina Georgiana Boboc <sup>1</sup>   
and Cristina Ileana Covaliu Mierla <sup>3</sup>

<sup>1</sup> National Institute for Research and Development in Environmental Protection, 294 Splaiul Independentei, 060031 Bucharest, Romania; dkrcontrol@yahoo.com (G.D.); lucianlaslo@yahoo.com (L.L.); monicamatei06@gmail.com (M.M.); mada91mada@yahoo.com (M.G.B.)

<sup>2</sup> Doctoral School of Biotechnical Systems Engineering, National University of Science and Technology POLITEHNICA of Bucharest, 060042 Bucharest, Romania

<sup>3</sup> Faculty of Biotechnical Systems Engineering, National University of Science and Technology POLITEHNICA of Bucharest, 060042 Bucharest, Romania; cristina\_covaliu@yahoo.com

\* Correspondence: natalia\_andreea92@yahoo.com

**Abstract:** This study emphasises the complexity of carbon dioxide (CO<sub>2</sub>) emission dynamics by conducting a wetland case study along the Dambovitza River. Our evaluation highlights the importance of considering spatial variability, meteorological parameters and water quality parameters. The variations in CO<sub>2</sub> emissions have been monitored using two complementary methods: a closed static chamber and a closed dynamic chamber. The closed dynamic chamber method has the highest level of confidence. The statistical results of correlations facilitated the validation of the closed static chamber method and its independent use in wetland ecosystems. Also, our findings revealed distinct patterns in emissions across locations that are influenced by parameters such as pH, redox potential (ORP), chlorophyll, dissolved oxygen concentration (DO), and temperature for the water–atmosphere interface. These results contribute to the understanding of the carbon cycle in wetlands and contribute to the improvement of greenhouse gas (GHG) reporting by obtaining data with a high level of confidence, regarding the role of wetland ecosystems in the carbon cycle.

**Keywords:** GHG inventory; chambers; climate change; temperature; water quality



**Citation:** Deák, G.; Enache, N.; Laslo, L.; Matei, M.; Boboc, M.G.; Covaliu Mierla, C.I. Water CO<sub>2</sub> Emission Monitoring in a Romanian Peri-Urban Wetland to Enhance GHG Reporting. *Atmosphere* **2024**, *15*, 1345. <https://doi.org/10.3390/atmos15111345>

Academic Editor: David F. Plusquellic

Received: 26 September 2024

Revised: 29 October 2024

Accepted: 7 November 2024

Published: 9 November 2024



**Copyright:** © 2024 by the authors. Licensee MDPI, Basel, Switzerland. This article is an open access article distributed under the terms and conditions of the Creative Commons Attribution (CC BY) license (<https://creativecommons.org/licenses/by/4.0/>).

## 1. Introduction

The increase in greenhouse gas (GHG) concentration in the atmosphere determines the amplification of the climate change phenomenon [1]. To limit the intensification of GHG emissions, measures have been taken since 1992, when the world's nations signed the United Nations Framework Convention on Climate Change—UNFCCC [2]. The UNFCCC sought to stabilise the GHG concentration in the atmosphere to allow ecosystems to adapt naturally to the impact of climate change. Starting in 1997, additional measures were taken through the Kyoto Protocol, which sets binding GHG reduction targets for developed countries that have signed this protocol. In 2015, the Paris Agreement was signed, with the first objective being to limit the increase in global mean temperature to 1.5–2 °C, above pre-industrial level. The Intergovernmental Panel on Climate Change (IPCC) is the United Nations body that has been appointed to assess scientific information on climate change. IPCC developed the methodology for the inventories of greenhouse gases generated by anthropogenic activities, depending on different key sectors [3,4]. These GHG inventories include the “Land Use, Land Use Change and Forestry” (LULUCF) sector, which covers emissions and removals from forest ecosystems, agricultural land, grasslands, settlements, and other lands, as well as wetland ecosystems [1]. The accumulation of carbon dioxide (CO<sub>2</sub>) in the atmosphere can be reduced through ecosystems by the accumulation of CO<sub>2</sub> in vegetation and soils, resulting in carbon sinks [5–9]. Human activities can affect

these reservoirs by changing land use, resulting in emissions or absorptions of atmospheric GHGs. The LULUCF sector can contribute to mitigating the effects of climate change by increasing the elimination of GHGs from the atmosphere or reducing emissions by stopping the loss of carbon stocks [10–13]. However, during the period 2007–2016, the IPCC working group characterised agriculture, forestry, and other land uses (AFOLU) as an important source of GHG emissions, contributing to approximately 23% of anthropogenic CO<sub>2</sub> emissions [2]. Soils can store large amounts of carbon (C), and some ecosystems can contain more C than all plant biomass [14,15]. The most important processes that affect the C balance of ecosystems are photosynthesis by surface vegetation, soil respiration and water respiration in the case of wetlands. The relationship between production and decomposition determines whether a system is a sink or a source of atmospheric CO<sub>2</sub> [16–18].

Wetlands encompass a diverse range of habitats and are characterised by the presence of water-saturated soils, situated at the transition between terrestrial and aquatic ecosystems. These ecosystems are among the most productive ecosystems on the planet, and they significantly influence the concentration of GHGs in the atmosphere, including CO<sub>2</sub>. Also, these are well known for their capacity to sequester and store carbon, primarily through the accumulation of organic matter in anaerobic conditions. However, wetlands also release substantial amounts of CO<sub>2</sub> into the atmosphere through various biogeochemical processes, contributing to GHG emissions and climate change [19].

A direct assessment of soil and water organic carbon involves field activities, such as carbon emission flux monitoring and soil and water sampling for laboratory analysis [20,21]. The application of high-tier methods recommended by the IPCC guidelines was targeted to improve GHG reporting for the LULUCF sector. Thus, for the application of superior tiers, it was necessary to obtain data with a high level of confidence, regarding the role of wetland ecosystems in the carbon cycle. In the present paper, the dynamics of carbon emission fluxes at three locations on the water surface were analysed, aiming to improve, on the one hand, the GHG inventories and, on the other hand, to establish sustainable management practises in wetland ecosystems [22–24].

Also, to accurately predict CO<sub>2</sub> emissions and assess the role of wetlands in the global carbon cycle, meteorological, physical and chemical parameters must be assessed. It is well known that temperature is a primary meteorological factor affecting microbial activity and organic matter decomposition rates, thereby influencing CO<sub>2</sub> emissions [25,26]. Soil moisture content is another critical parameter, with wetter conditions promoting anaerobic decomposition processes and subsequent CO<sub>2</sub> production. Additionally, precipitation patterns can influence soil moisture levels, indirectly impacting CO<sub>2</sub> emissions [27]. On the physicochemical side, pH levels influence the solubility of CO<sub>2</sub> in water and affect microbial community composition, thus modulating CO<sub>2</sub> production rates. Nutrient availability, such as nitrogen and phosphorus concentrations, can stimulate microbial activity and organic matter decomposition, amplifying CO<sub>2</sub> emissions [28,29]. The amount of dissolved organic matter, salinity, and conductivity may also change the dynamics of CO<sub>2</sub> by affecting the processes used by microbes and the rate at which carbon is recycled [30].

The establishment of GHG quantification methods and techniques for wetlands according to the requirements of the IPCC was identified and tested in pilot areas. The case study area along the Dâmbovița River, situated in the peri-urban area of Bucharest, allows a focused examination of CO<sub>2</sub> emissions in a rapidly urbanising region, especially at the transition between the river ecosystem and the accumulation lake. The presence of robust aquatic and riparian vegetation cover in areas near natural riverbanks contrasts with less dense vegetation in the transitional section, providing a varied dataset on how different vegetation densities affect CO<sub>2</sub> emissions. By developing and testing a methodology to estimate CO<sub>2</sub> emissions in this context, this research aims to provide insights that are applicable under similar meteorological conditions, improving the understanding of environmental impacts at urban–rural interfaces. In this research, the authors use two methods to analyse CO<sub>2</sub> emissions from the water–atmosphere interface and evaluated their performance to determine the most accurate CO<sub>2</sub> emissions. These methods include the dynamic closed

chamber method (EGM-5) and the static closed chamber method (Injection Kit) and were applied in a wetland case study in 2022. Unlike standard single-method approaches, which may offer limited accuracy, this novel dual approach cross-validates the results, ensuring a higher level of confidence in the data collected, especially in under-represented areas like peri-urban wetlands.

## 2. Materials and Methods

### 2.1. Site Description

The selected research area is localised in Romania's south-east part, in the peri-urban area of Bucharest, along the Dambovitza River, upstream from the "Lacul Morii" reservoir (Figure 1). Since the reservoir's construction in 1986, riverine wetlands have been formed upstream of it, covered by the specific vegetation of *Phragmites australis* and Cattails. The area considered in the case study has a perimeter of 8630 m and an area of 702,604 m<sup>2</sup>. Along with it, three locations (A, B, and C) were selected based on the spatial distribution and extent of vegetation to measure CO<sub>2</sub> emissions from the water's surface. Thus, location A, located upstream, is characterised by a narrow river course, with a naturally developed riverbed, and its banks are abundantly covered with Cattail vegetation. Location B features a more expansive riverbank than location A, a constructed riverbed, and dispersed mixed vegetation along the banks. This is considered an area of transition between points A and C in terms of vegetation distribution. Area C was selected for its positioning as close as possible to the constructed reservoir and also for the soils abundantly covered by *Phragmites australis* vegetation.

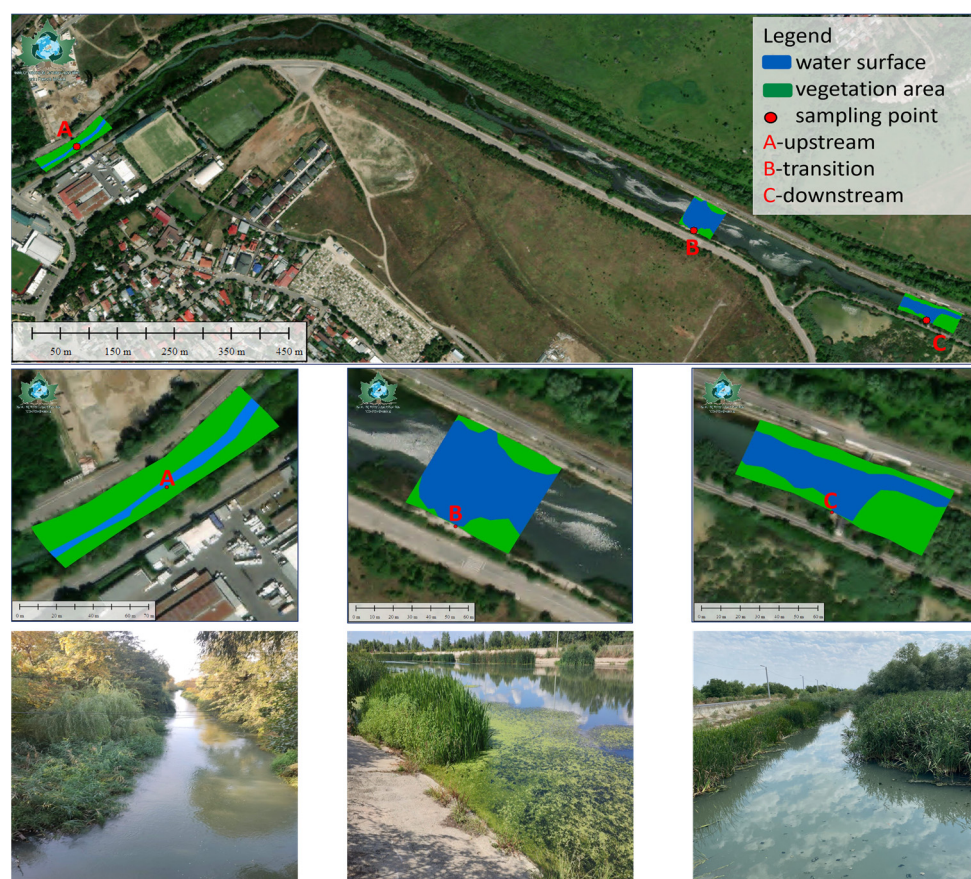


**Figure 1.** Spatial representation [31] and landscapes pictures of the measurement areas on the water surface.

## 2.2. Climatic Context

In Romania, the year 2022 ranks fourth in the list of the warmest years based on data from 129 weather stations between 1961 and 2023 (NMA, 2023) [32]. Bucharest was no exception to the warming trend; in 2022, positive thermal anomalies of up to 1.4 °C were recorded at the Bucharest–Afumati weather station compared to the standard reference period of 1991–2020. Moreover, on 24 July 2022, 40.7 °C was recorded at the Bucharest–Filaret meteorological station, the whole summer being characterised by persistent heat waves mainly in the southern and eastern regions of the country. Compared to the summer season, the spring of 2022 was mainly characterised by modest temperatures, close to the normal values for the period and atmospheric instability. Regarding the precipitations, they were predominantly excessive; in Bucharest, severe storms were registered, accompanied by blizzards and hail. The autumn season recorded above-normal temperatures in Bucharest; for example, on 2 November 2022, 25.6 °C was registered, 0.5 °C higher compared to the absolute maximum monthly temperature (10 November 2010). During the winter season, positive thermal anomalies were recorded; at the level of the entire country, the month of December of the year 2022 was the third warmest since 1961. In January 2022, positive air temperature anomalies of up to 2.8 °C were recorded, while in February, the value of the deviation reached up to 3.3 °C.

## 2.3. Field Sampling and Analyses

The main approach used to measure CO<sub>2</sub> emissions from the study area consisted of a method involving a closed dynamic and opaque chamber with a specific surface at the interface with water. Thus, a portable CO<sub>2</sub> gas analyser (EGM-5) was used to directly measure CO<sub>2</sub> emissions. This method is dynamic and measures the difference in CO<sub>2</sub> concentration (ppm) between the air entering and leaving the chamber by recirculating it. The main characteristics of the EGM-5 portable CO<sub>2</sub> gas analyser are its volume of 1171 mL and its covering area of 78 cm<sup>2</sup> [33]. To perform CO<sub>2</sub> emission measurements at the water–atmosphere interface, the equipment consisting of the EGM-5 analyser and the closed dynamic chamber, was specially adapted to the flooding conditions of aquatic ecosystems and was mounted on a floating device (Figure 2a) [19,21,29].



**Figure 2.** Field measurements with EGM-5 method on water (a) and the Injection Kit measurement method (b).

On the water's surface, continuous overlaid measurements were performed (without allowing the atmospheric air to enter the chamber) for 300 s each (the maximum allowed by the equipment), with the final value recorded after 15 min. The EGM-5 measurement data are provided in ppm; however, to ensure consistency with previous studies and related methods, the measurement unit is converted to g m<sup>-2</sup> h<sup>-1</sup> based on Equation (1) [33].

$$F_{\text{CO}_2} \left( \text{g m}^{-2} \text{h}^{-1} \right) = \frac{dC}{dT} \frac{\mu\text{mol}}{\text{mols}} \times \frac{P}{1013} \times \frac{273}{273 + T_{\text{air}}} \times \frac{44.009\text{g}}{22.414\text{dm}^3} \times \frac{V \text{ m}^3}{A \text{ m}^2} \times \frac{\text{mol}}{10^6 \mu\text{mol}} \times \frac{3600\text{s}}{\text{hr}} \times \frac{10^3\text{L}}{\text{m}^3} \quad (1)$$

where

$$\begin{aligned} \frac{dC}{dT} &= \text{concentration inside the chamber in time interval;} \\ \frac{P}{1013} &= \text{adjustment for barometric pressure with } P \text{ reported in millibar;} \\ \frac{273}{273+T_{air}} &= \text{air temperature adjustment;} \\ \frac{44.009\text{g}}{22.414\text{dm}^3} &= \text{molar volume and ideal gas constant at standard temperature and pressure;} \\ \frac{V}{A} &= \text{ratio between the chamber's volume and area.} \end{aligned}$$

An alternative to the closed dynamic chamber method that has been field-tested for determining emissions from the water–atmosphere interface is the Injection Kit method. This is a technique for measuring gas concentrations utilising small gas samples collected in a static chamber and transferred to the EGM-5 analyser by a syringe (Figure 2b). The Injection Kit consists of a network of tubes connected to a static chamber for CO<sub>2</sub> accumulation and a series of injections for gas sample collection. A static floating collection chamber with a volume of 4.25 L was used to collect CO<sub>2</sub> from the water–atmosphere interface.

This approach monitors CO<sub>2</sub> concentrations that accumulate in a closed opaque chamber placed on the surface of the water, and in this study, measurements were performed continuously for 30 min. During the first 5 min, samples were taken every 1 min, then repeated every 3 min, and the last two measurements were performed at each 5 min. The CO<sub>2</sub> concentration in the gas samples was calculated by injecting the sample into a fixed gas stream with a known CO<sub>2</sub> concentration. Then, we measured the CO<sub>2</sub> sample collected from atmospheric air and calculated the difference in value between the initial or atmospheric concentration and the concentration of CO<sub>2</sub> from the sample [34]. CO<sub>2</sub> emissions were calculated and converted from the mixing ratio (ppm) to mass units according to Equation (2) by assuming a model of the relation between gas concentration and time interval [19].

$$f \left( \text{g m}^{-2} \text{ h}^{-1} \right) = 10^{-3} \frac{V}{A} \frac{dCO_2}{dt} \frac{MP}{R(273.15 + T)} \quad (2)$$

where

$$\begin{aligned} \frac{V}{A} &= \text{the ratio between the chamber's volume and area;} \\ \frac{dC}{dT} &= \text{the change in concentration in time;} \\ M &= \text{molar mass of CO}_2 \text{ (g/mol);} \\ P &= \text{air pressure (atm);} \\ R &= \text{ideal gas constant (0.0821 L atm /mol K);} \\ T &= \text{air temperature (}^\circ\text{C).} \end{aligned}$$

Both methods of measuring CO<sub>2</sub> emission fluxes were applied in situ in the research area during the year 2022, with measurement sessions occurring at least once a month for water–atmosphere interface assessments. Although the two methods, which operate with opaque chambers, are complementary, the EGM-5 method is considered reference one since it is the most accurate. Both methods present limitations in determining net emissions and do not allow the measurement of CO<sub>2</sub> uptake in ecosystems.

#### 2.4. Monitoring the Key Parameters That Influence CO<sub>2</sub> Emissions

To evaluate the parameters on which CO<sub>2</sub> emissions depend, field measurements, laboratory analyses and weather data collection were carried out, using conventional methods to determine the evolution of each variable. The meteorological parameters classified as factors that deeply affect or even regulate CO<sub>2</sub> exchanges at the water–atmosphere interface are air temperature ( $T_{air}$ ), precipitation (Pp) and wind speed [35]. The temperature values at 2 m and pressure data are satellite data collected from the NASA POWER [36] platform's precipitation measurement campaign.

To further emphasise the impact of precipitation on CO<sub>2</sub> emissions, it was investigated if this effect is amplified or takes effect over time, and thus, the correlation of CO<sub>2</sub> emissions with cumulative precipitation over three days was chosen for emissions from the water–atmosphere interface.

Field experiments involved the measurements of physical parameters such as air temperature ( $T_{\text{air}}$ ) and water temperature ( $T_{\text{water}}$ ), water pH and water quality analyses.  $T_{\text{water}}$  and water pH were determined in situ, simultaneously, with the same multiparametric measuring instrument, Lutron PH222 ( $\pm 0.05$  pH). The physical–chemical parameters of the water were measured in situ using a calibrated Eureka Manta 2 multiparametric water quality probe. Two series of measurements were conducted on the same plot to determine the concentration distribution of measured parameters such as pH, chlorophyll, salinity, dissolved oxygen concentration (DO), redox potential (ORP), conductivity, turbidity, water temperature, total dissolved solids (TDS), and chromophoric dissolved organic matter (CDOM).

To determine the water quality parameters, water samples were collected in May from each plot. The water samples were analysed for pH parameters, key nutrients such as nitrogen (N) and phosphorus (P), chemical oxygen demand (COD), and chlorophyll-a.

Carbon dioxide emissions are influenced by multiple factors directly or indirectly [37]. For the analysis of the effect of these parameters on the  $\text{CO}_2$  emission variability, the Pearson analysis was used. Likewise, simple and multiple regression analyses were used to test and validate  $\text{CO}_2$  emission models appropriate to the study areas. For the entire factorial analysis process, statistical analysis software (SPSS) 29.0 was used.

### 3. Results

The measurement campaign included the monitoring of potential  $\text{CO}_2$  emissions from the reservoir, Lacul Morii. Weekly measurements were conducted over the summer season, when respiration should be at its peak, but the emission values recorded were predominantly negative, ranging from  $-4.18 \text{ g m}^{-2} \text{ h}^{-1}$  to  $-0.11 \text{ g m}^{-2} \text{ h}^{-1}$ . These results demonstrate the existence of carbon sequestration conditions, and, according to the IPCC, it has been confirmed that the lake no longer emits  $\text{CO}_2$  25 years after its construction [1]. Further, the hypothesis that  $\text{CO}_2$  flux upstream may vary due to a range of factors has been researched. Thus,  $\text{CO}_2$  emissions were measured and assessed in riverine wetlands formed upstream of the reservoir at the water–atmosphere interface.

#### 3.1. Physicochemical Characterisation of the Water in Each Investigated Location

To characterise the water quality at each research location, laboratory analyses of the main water quality indicators were performed. The results of the water samples collected from the three locations established along the river’s course are presented in Table 1.

**Table 1.** Physicochemical indicators of water characteristic of each study location.

Indicator		A	B	C
pH	pH (t °C)	7.54 (21.4)	7.36 (21.8)	7.39 (22.1)
$N_{\text{total}}$	mg N/L	3.92	4.20	8.40
$P_{\text{total}}$	mg P/L	0.123	0.243	0.333
COD	mg $\text{O}_2$ /L	5.98	15.3	9.4
Chlorophyll-a	$\mu\text{g/L}$	1.18	4.74	3.55

The value of the pH in location A indicates that the water is slightly alkaline. Considering that wastewater is discharged upstream, this might explain why this location has a higher pH. Also, this location exhibits relatively low levels of both total nitrogen and total phosphorus. The low COD values suggest the influence of anthropogenic activities in the area, but the chlorophyll-a values indicate a relatively healthy aquatic ecosystem with moderate primary productivity.

The value of the pH in location B is lower than that in location A and is most likely caused by the increase in total nitrogen and total phosphorous content. Higher levels of COD suggest possible pollution, likely from urban runoff or wastewater discharge; nevertheless, despite these high levels, the location exhibits increased primary production, most likely because of nutrient input. As a response to nutrient enrichment due to

pollution or other factors, there might be the periodic presence of floating masses on the water surface developed by *Spirogyra* species identified in this study location during the monitoring period.

The pH value of the water in location C indicates that it is also slightly acidic. However, this area exhibits significantly elevated levels of both total nitrogen and total phosphorus. The total nitrogen value of 8.40 mg N/L indicates a high concentration of nitrogen compounds, and the total phosphorus value of 0.333 mg P/L suggests a relatively high concentration, which can exacerbate eutrophication issues, leading to algal blooms, oxygen depletion, and negative impacts on this aquatic ecosystem. This area may be under ecological stress from upstream chromium pollution, but the relatively moderate levels of both COD and chlorophyll-a suggest that the ecosystem may still be resilient.

### 3.2. Extrapolation of CO<sub>2</sub> Emissions

The extrapolation of CO<sub>2</sub> emissions in 2022 based on air temperature and pressure (Table S1) for the study area involves the unobserved values of CO<sub>2</sub> emissions using the model adapted to the in situ measured data.

Table S2 provides data, including the mean CO<sub>2</sub> emissions, standard deviations (SDs), and 95% confidence intervals for each month. The extrapolated mean CO<sub>2</sub> emission rate of location A shows significant variation throughout the year. The lowest calculated mean is in February with 0.605 g m<sup>-2</sup> d<sup>-1</sup> for EGM-5 and 0.769 g m<sup>-2</sup> d<sup>-1</sup> for the Injection Kit, and the peak is for EGM-5 in June with 21.744 g m<sup>-2</sup> d<sup>-1</sup> and for the Injection Kit in August, with values of 14.810 g m<sup>-2</sup> d<sup>-1</sup>. EGM-5 has a peak of emissions for location B in July when the extrapolated values are 3.473 g m<sup>-2</sup> d<sup>-1</sup> and are lowest in December (0.374 g m<sup>-2</sup> d<sup>-1</sup>). The values obtained by the Injection Kit method had the maximum average of CO<sub>2</sub> extrapolated emissions in August, with 3.315 g m<sup>-2</sup> d<sup>-1</sup> and the lowest, also in December, with 0.265 g m<sup>-2</sup> d<sup>-1</sup>. This location has low variability in emissions, except in the summer season. For location C, the highest emissions occurred in August for both methods, with 2.153 g m<sup>-2</sup> d<sup>-1</sup> and 1.767 g m<sup>-2</sup> d<sup>-1</sup>, respectively, and the lowest in January, with 0.214 g m<sup>-2</sup> d<sup>-1</sup> and 0.165 g m<sup>-2</sup> d<sup>-1</sup>. Confidence intervals are generally narrow, indicating precise estimates for most months. The values of the confidence coefficient for this extrapolation indicate that between 64.35% and 67.56% of the variability of CO<sub>2</sub> emission measurements is due to real differences, the rest of the percentage difference being attributed to errors determined by the non-uniform frequency of measurement campaigns or other factors.

To better reflect the real CO<sub>2</sub> emissions in extrapolation, the average monthly CO<sub>2</sub> emissions were corrected and adjusted, considering the differences in emissions between day and night. The confidence coefficients of these values were also determined (Table 2). The adjustment values highlight significant seasonal variations and provide more accurate estimates. Location A shows the most significant difference in values, where the corrected mean for EGM-5 in June is 36.240 g m<sup>-2</sup> d<sup>-1</sup> and 21.808 g m<sup>-2</sup> d<sup>-1</sup> for the Injection Kit, with a confidence coefficient of 73.29%, compared to the initial uncorrected mean of 21.744 g m<sup>-2</sup> d<sup>-1</sup> and 13.047 g m<sup>-2</sup> d<sup>-1</sup>, respectively. For location B, the corrected means range from 0.253 g m<sup>-2</sup> d<sup>-1</sup> to 6.940 g m<sup>-2</sup> d<sup>-1</sup> for EGM-5 and from 0.160 g m<sup>-2</sup> d<sup>-1</sup> to 3.926 g m<sup>-2</sup> d<sup>-1</sup>, with confidence coefficients consistently at 73.27% or 73.29%. This suggests moderate confidence in measurements across the months. For location C, the corrected means vary less for both methods, from 0.153 g m<sup>-2</sup> d<sup>-1</sup> to 3.468 g m<sup>-2</sup> d<sup>-1</sup> for EGM-5 and from 0.118 g m<sup>-2</sup> d<sup>-1</sup> to 2.372 g m<sup>-2</sup> d<sup>-1</sup> with the Injection Kit, with confidence coefficients also consistently at 73.27% or 74.03%. This location shows lower variability in mean values but still maintains a similar level of confidence.

**Table 2.** Extrapolated mean CO<sub>2</sub> emissions for each location, based on the hypothesis that considers the day and night variation.

Location Method Month	A			B			C		
	EGM-5 Corrected Mean	Injection Kit Corrected Mean	Confidence Coefficient	EGM-5 Corrected Mean	Injection Kit Corrected Mean	Confidence Coefficient	EGM-5 Corrected Mean	Injection Kit Corrected Mean	Confidence Coefficient
January	1.560	0.862	73.27%	0.777	0.562	74.03%	0.153	0.118	73.27%
February	0.512	0.654	76.88%	1.816	0.652	76.88%	0.672	0.459	76.88%
March	4.572	5.484	73.27%	1.212	0.773	73.27%	0.960	0.658	74.03%
April	6.053	4.870	73.29%	1.443	1.092	73.29%	1.112	0.871	73.29%
May	12.288	9.411	74.03%	4.184	1.767	74.03%	2.382	1.724	74.03%
June	36.240	21.808	73.29%	6.204	3.808	73.29%	3.468	2.360	73.29%
July	19.683	8.279	73.27%	5.993	3.427	73.27%	2.829	2.372	73.27%
August	24.444	17.503	73.27%	6.940	3.926	73.27%	2.544	2.093	73.27%
September	4.997	10.615	73.29%	4.901	1.080	73.29%	0.864	1.301	73.29%
October	2.522	1.466	73.27%	0.762	0.658	73.27%	0.717	0.463	74.03%
November	0.962	1.245	75.67%	0.631	0.513	75.67%	0.237	0.274	74.88%
December	1.320	1.153	74.80%	0.253	0.160	74.03%	0.497	0.485	74.80%

3.3. Analysis of Seasonal Variability of CO<sub>2</sub> Emissions from the Water–Atmosphere Interface

Figure 3 illustrates the local climate–temperate seasonal variability of CO<sub>2</sub> emissions at the water–atmosphere interface, measured by the EGM-5 method. In general, all three locations showed clear seasonal patterns of CO<sub>2</sub> emissions during the growing season, with the highest levels observed in the summer and the lowest in the winter. This pattern indicates that higher summer temperatures significantly enhance biological activity and soil respiration, leading to higher CO<sub>2</sub> emissions, whereas the colder winter months suppress these processes. Location A exhibits the most significant rise in summer emissions, with larger variability compared to the other seasons, reaching 24.444 g m<sup>−2</sup> d<sup>−1</sup>, which indicates a pronounced temperature sensitivity. Spatial variations are also evident between the three study locations; thus, compared to location A, locations B and C consistently show lower emissions in all seasons, reaching a peak during summer at 6.940 g m<sup>−2</sup> d<sup>−1</sup>, respectively, and 3.468 g m<sup>−2</sup> d<sup>−1</sup> in spring, which also indicates the influence of site-specific environmental factors in CO<sub>2</sub> dynamics.

Table 3 summarises the performance metrics and equations of regression models using temperature and pressure as parameters. The parameters are analysed based on their correlation (R<sup>2</sup>), regression equations (Eq.), and standard deviation (SD) of the residuals. The regression results for the T<sub>air</sub> parameter indicate that the proportion of variance explained by the model is the most significant for location B, where R<sup>2</sup> = 0.926. This location has the lowest SD (0.996), indicating the predictions are closest to the actual values. Also, locations A and C show positive and significant correlation coefficients, with R<sup>2</sup> = 0.872 and R<sup>2</sup> = 0.851, respectively. The coefficient of determination for pressure in the three locations indicates that the proportion of variation is also highest in location B, where R<sup>2</sup> = 0.927, but is also significant in location A with R<sup>2</sup> = 0.843, and location C with R<sup>2</sup> = 0.851. Multiple regression shows a decrease in R<sup>2</sup> values compared to a single parameter; thus, location B has an R<sup>2</sup> of 0.837, location A has 0.671, and in location C, it is statistically insignificant.

**Table 3.** Regression models between CO<sub>2</sub> emissions measured with EGM-5 and meteorological parameters in the investigated locations.

Regression Model	Statistical Parameters	Location A	Location B	Location C
Simple regression $E = f(T)$	R <sup>2</sup>	0.8728	0.926	0.851
	Eq.	$y = 0.02445T^{2.12}$	$y = 0.03984T^{1.56}$	$y = 0.04516T^{1.26}$
	SD	6.454	0.996	0.617
Simple regression $E = f(P^*)$	R <sup>2</sup>	0.843	0.927	0.851
	Eq.	$y = 5.467 \times 10^4 P^{2.1}$	$y = 1.894 \times 10^3 P^{1.55}$	$y = 2.721 \times 10^2 P^{1.255}$
	SD	6.447	0.989	0.617
Multiple regression $E = f(T, P^*)$	R <sup>2</sup>	0.671	0.837	0.397
	Eq.	$E = 233.7 + 0.788T - 233.8P$	$E = -0.557 - 1.012T + 1.282 \times 10^3 P$	$E = -11.33 + 0.266T + 10.59P$
	SD	6.312	1.123	3.418

P\* = P/1000.



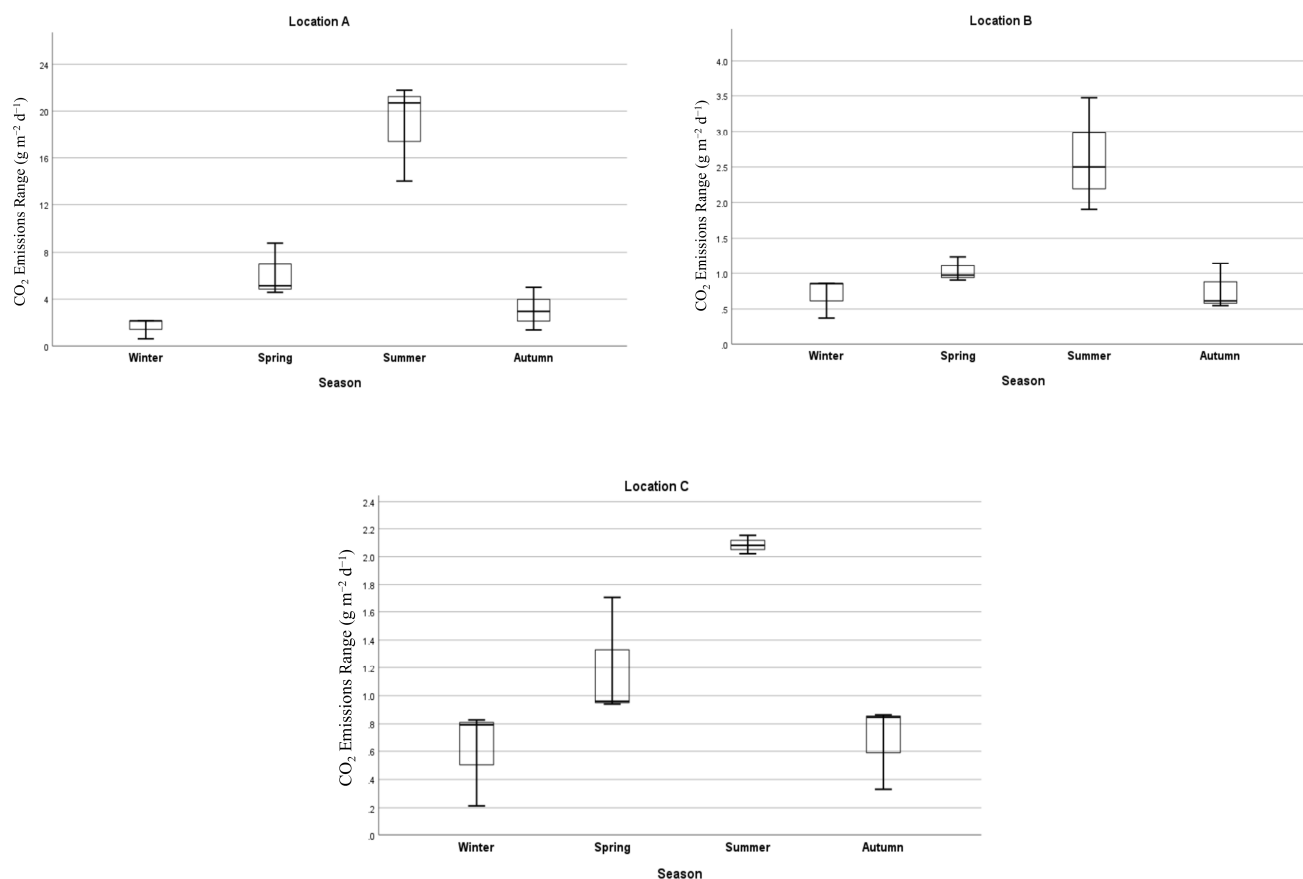


**Figure 3.** Seasonal variability of CO<sub>2</sub> emissions from water–atmosphere interface measured by EGM-5 method.

The box plots from Figure 4 illustrate seasonal CO<sub>2</sub> emissions across the three locations measured using the Injection Kit method. The CO<sub>2</sub> emissions also show, in the case of this method, clear seasonal variation, with summer consistently exhibiting the highest emissions in all locations. In location A, emissions exhibit a dramatic increase in the summer season, reaching a peak between 17.503 g m<sup>-2</sup> d<sup>-1</sup> and 21.808 g m<sup>-2</sup> d<sup>-1</sup>, whilst winter values are at their lowest, ranging from 0.654 g m<sup>-2</sup> d<sup>-1</sup> to 1.153 g m<sup>-2</sup> d<sup>-1</sup>. This trend suggests that, in location A, the intense biological activity due to the presence of abundant vegetation in the warmer months leads to the increased release of CO<sub>2</sub> [38]. Location B, on the other hand, shows a more subdued response in CO<sub>2</sub> emissions compared to location A, with lower overall emissions throughout the year. While summer still shows the highest emissions between 3.427 g m<sup>-2</sup> d<sup>-1</sup> and 3.926 g m<sup>-2</sup> d<sup>-1</sup>, the difference between seasons is less pronounced, with winter and spring being similar. In location C, the pattern is more complex, with significant variation between seasons as spring experiences a substantial rise in emissions up to 1.724 g m<sup>-2</sup> d<sup>-1</sup>, while for winter, it remains low, with CO<sub>2</sub> emissions ranging from 0.118 g m<sup>-2</sup> d<sup>-1</sup> to 0.485 g m<sup>-2</sup> d<sup>-1</sup>, similar to location B. Notably, summer emissions are more stable at location C, indicating that the warm season in this location might not have as dramatic an impact on CO<sub>2</sub> release. Autumn, however, sees a decline, but emissions remain elevated compared to winter.

The regression models applied for emissions measured with the Injection Kit method demonstrated strong predictive capabilities based on temperature and pressure across the three locations, as indicated in Table 4. Simple regressions for temperature showed the highest R<sup>2</sup> values in Location B, with R<sup>2</sup> = 0.933, indicating that temperature alone accounts for most of the emission variation. Location C follows with R<sup>2</sup> = 0.851, while location A is slightly lower but still very strong with R<sup>2</sup> = 0.842. The non-linear equations reveal location-specific differences in the sensitivity of emissions to temperature and pressure.

The SD for these simple regressions indicates that location C offers the most accurate emissions predictions, whereas location A exhibits higher variability. The coefficient of determination for pressure demonstrates strong predictive power, with Location B again showing the highest  $R^2 = 0.925$ . The equations indicate non-linear relationships between emissions and pressure, where the SD revealed that location C has the lowest prediction error, making it the most reliable, while location A has the highest variability. When considering both temperature and pressure in multiple regression models, the performance remains strong, particularly in location C, where  $R^2 = 0.869$ , followed by location B with  $R^2 = 0.750$ , indicating a robust combined effect of the two variables. Location A shows a weaker fit with  $R^2 = 0.660$ , suggesting higher uncertainty in these predictions.

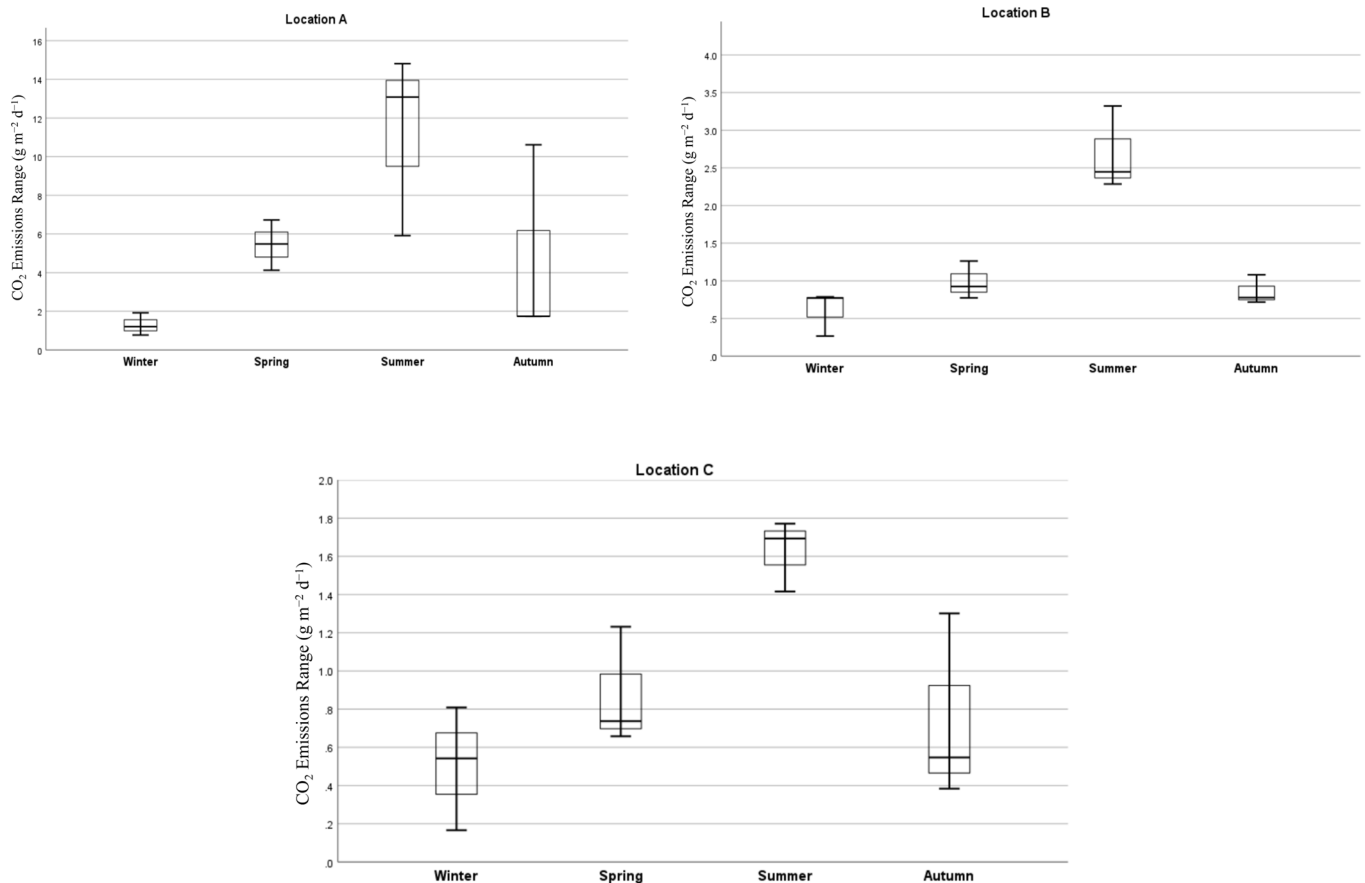


**Figure 4.** Seasonal variability of CO<sub>2</sub> emissions from water–atmosphere interface measured by Injection Kit method.

**Table 4.** Regression models between CO<sub>2</sub> emissions measured with Injection Kit and meteorological parameters in investigated locations.

Regression Model	Statistical Parameters	Location A	Location B	Location C
Simple regression $E = f(T)$	$R^2$	0.842	0.933	0.851
	Eq.	$E = 5.214 \times 10^{-2}T^{1.6}$	$E = 0.221T^{1.211}$	$E = 0.5215T^{0.068}$
	SD	2.309	0.803	0.646
Simple regression $E = f(P^*)$	$R^2$	0.842	0.925	0.793
	Eq.	$E = 3.324 \times 10^3P^{1.599}$	$E = 4.969 \times 10^4P^{2.509}$	$E = 1.179 \times 10^2P^{1.005}$
	SD	2.305	0.845	0.751
Multiple regression $E = f(T,P^*)$	$R^2$	0.660	0.750	0.869
	Eq.	$E = 0.133T + 2.091P$	$E = 0.104T + 0.606P$	$E = 0.44T + 0.837P$
	SD	3.200	1.199	0.631

$P^* = P/1000$ .

### 3.4. Drivers of CO<sub>2</sub> Emission Variability: Meteorological Parameters

The following graphs show the daily mean values of CO<sub>2</sub> emissions measured with the EGM-5 method (Figure 5a) and with the Injection Kit method (Figure 5b) in relation to the variable T<sub>air</sub> for each location. The variation in CO<sub>2</sub> emissions follows similar trends to those of temperatures; thus, higher emissions are observed in all three locations in the vegetation season between June and August. Lower emissions were measured in winter (December, January, and February) when the minimum T<sub>air</sub> reached −4.11 °C and also in late autumn. The intra-annual variations in CO<sub>2</sub> emissions from location C have an oscillating trajectory, and major discrepancies between them and T<sub>air</sub> are evident in the warm season. This might be due to microbial activity, plant photosynthesis, or dynamic hydrological processes due to the proximity of this location to the reservoir [39,40].

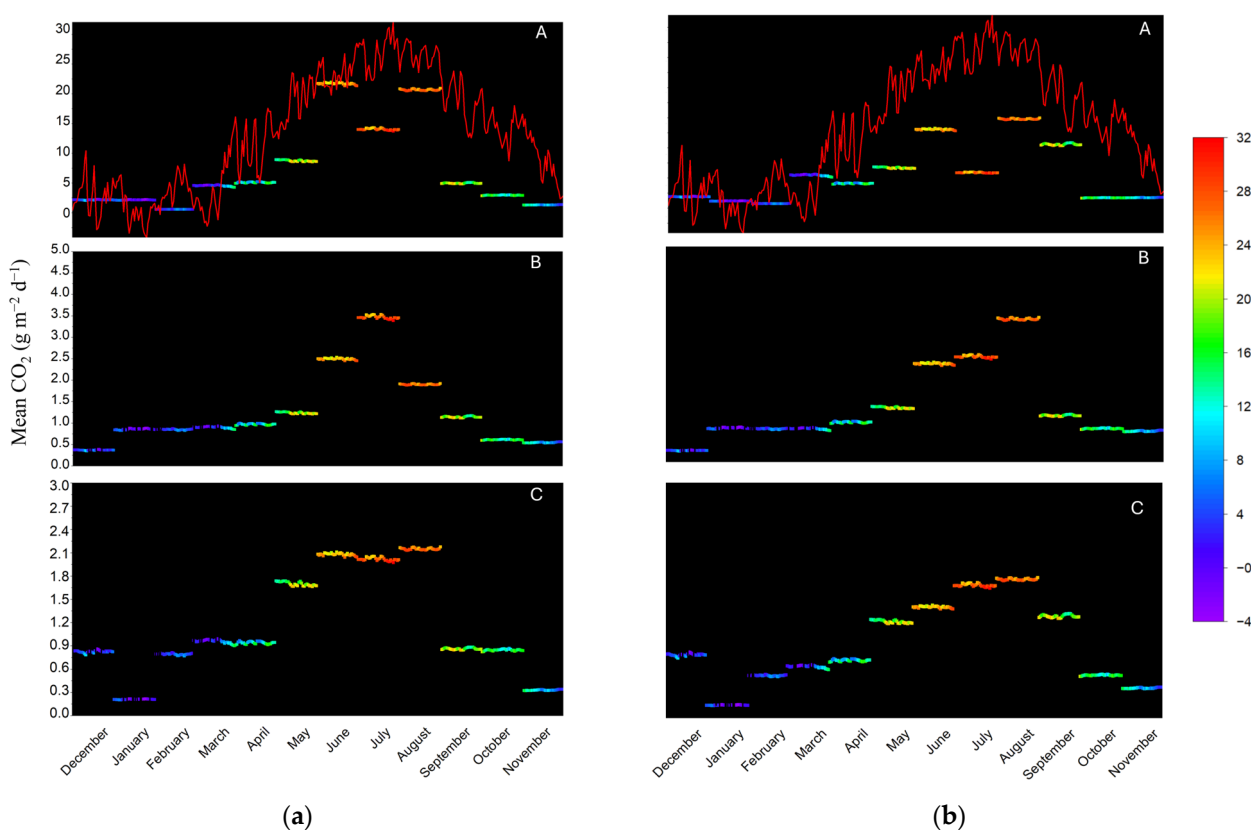


**Figure 5.** Variation in monthly average CO<sub>2</sub> emissions measured with the EGM-5 (a) and Injection Kit (b) method and daily mean air temperature.

Pearson product correlations were further employed to investigate correlations between meteorological factors and CO<sub>2</sub> emissions as the dependent variables. A matrix of correlation coefficients between the independent variables and CO<sub>2</sub> emissions from each location is presented in Table 5.

According to the correlation matrices for all three locations analysed, only temperatures had a positive and significant influence on CO<sub>2</sub> emissions based on the values gathered and assessed from a statistical standpoint.

The Pearson product correlation between the EGM-5 and Injection Kit methods with T<sub>air</sub> proved to be strongly positive and statistically significant [41] in location A, with  $r = 0.676$  ( $p < 0.01$ ) and  $r = 0.598$  ( $p < 0.01$ ), respectively, and in location B, with  $r = 0.832$  ( $p < 0.01$ ) and  $r = 0.734$  ( $p < 0.01$ ), respectively, while in location C, they showed similarities in significance, with  $r = 0.738$  ( $p < 0.01$ ) and  $r = 0.777$  ( $p < 0.01$ ), respectively.

**Table 5.** Correlation matrix showing Pearson correlation coefficient for CO<sub>2</sub> emissions and meteorologic parameters for locations A, B and C.

Location		EGM-5	Injection Kit	T <sub>air</sub>	T <sub>water</sub>	Wind Speed	Cumulative Pp
A	EGM-5	1					
	Injection Kit	0.862 **	1				
	T <sub>air</sub>	0.676 **	0.598 **	1			
	T <sub>water</sub>	0.788 **	0.661 **	0.892 **	1		
	Wind Speed	−0.032	−0.311	0.033	−0.095	1	
	Cumulative Pp	−0.514	−0.309	−0.806	−0.66	0.046	1
B	EGM-5	1					
	Injection Kit	0.812 **	1				
	T <sub>air</sub>	0.832 **	0.734 **	1			
	T <sub>water</sub>	0.793	0.643 **	0.957 **	1		
	Wind Speed	−0.007	−0.197	−0.063	−0.063	1	
	Cumulative Pp	−0.181	−0.351	−0.347	−0.368	0.383	1
C	EGM-5	1					
	Kit	0.785 **	1				
	T <sub>air</sub>	0.738 **	0.777 **	1			
	T <sub>water</sub>	0.677 **	0.685 **	0.973 **	1		
	Wind Speed	0.093	−0.091	−0.09	−0.16	1	
	Cumulative Pp	−0.311	−0.249	−0.388	−0.497	0.018	1

\*\* Correlation is significant at the 0.01 level (1-tailed).

There were also significant, positive correlations between the EGM-5 and Injection Kit methods with T<sub>water</sub> in location A, with  $r = 0.788$  ( $p < 0.01$ ) and  $r = 0.661$  ( $p < 0.01$ ), in location B, with  $r = 0.793$  ( $p < 0.01$ ) and  $r = 0.643$  ( $p < 0.01$ ), and in location C, where the Person product correlation value was  $r = 0.677$  ( $p < 0.01$ ) for the EGM-5 method and  $r = 0.685$  ( $p < 0.01$ ) for the Injection Kit method.

### 3.5. Comparison Between and Validation of the Two Complementary Methods

Figure 6 shows the temporal variability of the CO<sub>2</sub> emissions monitored with the EGM-5 method and the Injection Kit method depending on the spatial variability. Throughout the monitoring period, in location A, the mean CO<sub>2</sub> emissions measured with EGM-5 ranged between  $0.02176 \text{ g m}^{-2} \text{ d}^{-1}$  in November and  $0.9963 \text{ g m}^{-2} \text{ d}^{-1}$  in August. The Injection Kit method highlighted average monthly values of CO<sub>2</sub> emissions between  $0.00906 \text{ g m}^{-2} \text{ d}^{-1}$  also in November and  $0.5823 \text{ g m}^{-2} \text{ d}^{-1}$  in August. In this location, the variation in the monthly amplitude between the two methods was a maximum of  $0.6959 \text{ g m}^{-2} \text{ d}^{-1}$  in June, and the average difference between the two methods for this location was  $0.0734 \text{ g m}^{-2} \text{ d}^{-1}$ . The Pearson correlation coefficient between the two methods for location A was found to be strongly positive and statistically significant [41] ( $r = 0.862$ ;  $p < 0.01$ ). Location B had higher discrepancies in the values of CO<sub>2</sub> emissions obtained by the two methods, with an average of the differences throughout the entire monitoring period of  $0.0914 \text{ g m}^{-2} \text{ d}^{-1}$ , whereas location C had an average of  $0.0491 \text{ g m}^{-2} \text{ d}^{-1}$ . The Pearson correlation coefficient between the two methods for both location B and location C proved to be strongly positive and statistically significant, with  $r = 0.812$ ;  $p < 0.01$  and  $r = 0.785$ ;  $p < 0.01$ . Although the monthly averages show the same trend of CO<sub>2</sub> emission values measured with both methods, with the Pearson correlation coefficient being strongly positive and statistically significant [41], significant differences appear in conditions of increased CO<sub>2</sub> emissions.

The difference between the magnitude of the recorded values may be due to the fundamental principles of each method, with the EGM-5 method having a closed chamber equipped with a pump that recirculates the gas, while the Injection Kit employs a closed chamber in which the gas accumulates.

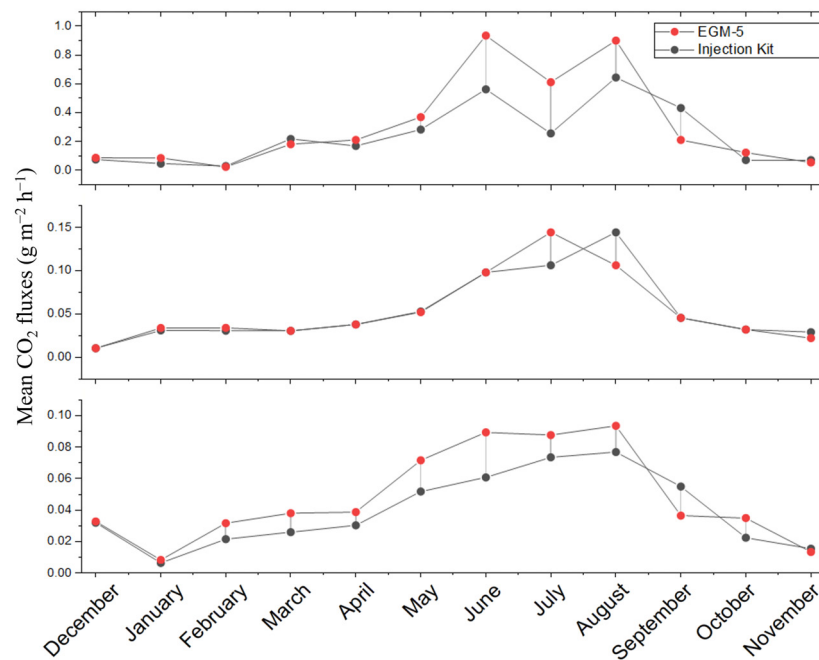


**Figure 6.** Analysis of the variability of CO<sub>2</sub> emissions obtained in locations A, B and C.

To highlight the importance of understanding CO<sub>2</sub> emissions from the water–atmosphere interface along the study area, and to obtain highly accurate monitoring results, two complementary methods, the EGM-5 method and the Injection Kit technique, were utilised in situ and compared. Thus, the boxplot graph in Figure 7 illustrates the CO<sub>2</sub> emission ranges based on measurements performed in each month for both methods, as well as their variations over time. For each location, the EGM-5 method consistently shows higher median and mean CO<sub>2</sub> fluxes compared to the Injection Kit, along with greater variability and more outliers, indicating that EGM-5 captures a wider range of CO<sub>2</sub> emission rates. The Injection Kit method, in contrast, demonstrates lower and more consistent CO<sub>2</sub> emission values with narrower interquartile ranges and fewer outliers. This suggests that the Injection Kit provides more stable and lower estimates of CO<sub>2</sub> fluxes, while the EGM-5 method detects higher and more variable fluxes under the same conditions.

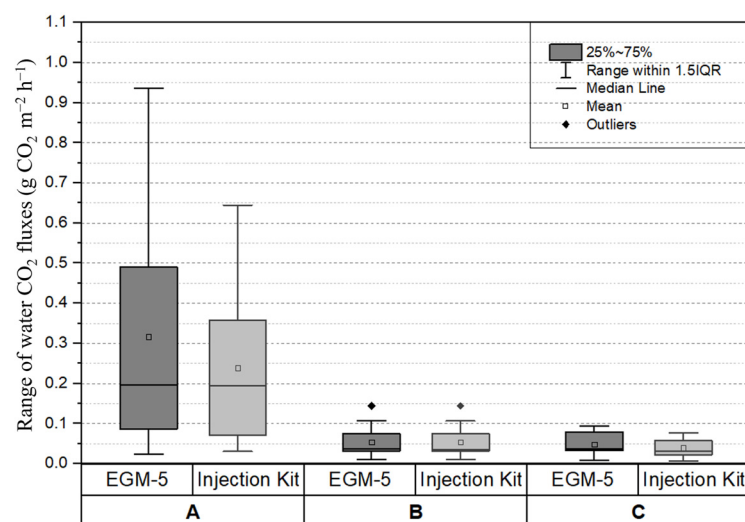


**Figure 7.** Analysis of the variability of CO<sub>2</sub> emissions obtained through the study area by utilising the EGM-5 and Injection Kit method over a year.

### 3.6. Effect of Water Quality on CO<sub>2</sub> Emissions

For a more precise explanation of the emissions from the water–air surface, the values of the water quality parameters in each study location were involved. Thus, correlation of the Pearson product, as well as linear regressions, were used for statistical analysis, both for the entire research area and for each location (Tables S3 and S4). These aims determine the spatial level of CO<sub>2</sub> emission correlations by calculating the values of the correlation coefficients employing both methods used in the measurements, as well as the degree of significance and linear relationship between CO<sub>2</sub> emissions and water quality parameters.

Thus, the correlation values show that variables such as pH, conductivity, salinity and TSD tend to have negative correlations with CO<sub>2</sub> emissions measured with the EGM-5 method, while ORP, DO%, CDOM, turbidity and DO mg/L show positive correlations. For location A, there are strong negative correlations [41] with pH ( $r = -0.820$ ;  $p < 0.01$ ), while ORP ( $r = 0.700$ ;  $p < 0.01$ ), chlorophyll ( $0.813$ ;  $p < 0.01$ ) and DO ( $r = 0.748$ ,  $p < 0.01$ ) show strong positive correlations [41]. The regression coefficients indicate the highest significance in location A for pH, where  $R^2 = 0.836$ ;  $p < 0.01$ , meaning that 83.6% of the variance in emissions measured by EGM-5 was predictable from the level of pH. In location B, most variables showed weak correlations with CO<sub>2</sub> emissions, except for pH which had moderate negative correlations ( $r = -0.619$ ;  $p < 0.01$ ), while chlorophyll proved to have a positive correlation ( $r = 0.681$ ;  $p < 0.01$ ). The regression coefficients were found to be significant for all the water quality parameters analysed. In location C, pH ( $r = -0.910$ ;  $p < 0.01$ ) and turbidity ( $r = -0.955$ ;  $p < 0.01$ ) had negative correlations, while ORP ( $r = 0.854$ ;  $p < 0.01$ ), chlorophyll ( $r = 0.946$ ;  $p < 0.01$ ) and DO% ( $r = 0.692$ ;  $p < 0.01$ ), had positive correlations. The bivariate regression equations showed a significance of the regression coefficient for pH ( $R^2 = 0.829$ ;  $p < 0.01$ ), chlorophyll ( $R^2 = 0.895$ ;  $p < 0.01$ ), DO% ( $R^2 = 0.805$ ;  $p < 0.01$ ) and turbidity, respectively, where  $R^2 = 0.911$ ;  $p < 0.01$ .

CO<sub>2</sub> emissions assessed using the Injection Kit method reveal a similar pattern of correlations with variables analysed at the entire study area level. For instance, pH displays negative correlations, whereas DO% shows positive correlations, albeit with strong variations. Location A stands out with positive correlations between CO<sub>2</sub> emissions and variables like chlorophyll ( $r = 0.632$ ;  $p < 0.01$ ) and DO mg/L ( $r = 0.737$ ;  $p < 0.01$ ), highlighting the influence of these factors on carbon release in this specific context. Location B, on the other hand, has weaker and more inconsistent correlations, highlighting the complexities of the relationship between environmental variables and CO<sub>2</sub> emissions. Location C exhibits a mix of both negative and positive correlations; thus pH ( $r = 0.765$ ;  $p < 0.01$ ) and turbidity ( $r = -0.822$ ;  $p < 0.01$ ) present negative correlations with CO<sub>2</sub> emissions, while chlorophyll ( $r = 0.775$ ;  $p < 0.01$ ) and DO% ( $r = 0.808$ ;  $p < 0.01$ ) show positive correlations, with high degrees of strength. Additionally, ORP displays a modest positive correlation with CO<sub>2</sub> emissions. Bivariate regression analysis was also applied to determine a significant portion of the variability in the CO<sub>2</sub> emission measured by the Injection Kit that can be attributed to changes in the independent variables. In location C, turbidity has an  $R^2$  of 0.853, indicating that 85.2% of the variance in the dependent variable is explained by turbidity, suggesting a very strong negative correlation [41]. Similarly, DO% in location C has an  $R^2$  of 0.838, showing a very strong positive correlation [41]. These high  $R^2$  values highlight the importance of turbidity and DO% in explaining the variance in the dependent variable at this location. Conversely, lower  $R^2$  values were obtained in locations A and B, indicating weaker explanatory power.

The Injection Kit method reveals similar patterns of correlations. Even if some variables consistently correlate with CO<sub>2</sub> emissions across both methods, the Injection Kit method usually indicates weaker correlations than the EGM-5 method. The effects of water quality variables are complex and often interconnected. Also, regression analysis for each variable revealed the complexities of these relations, emphasising the importance of complex location-specific solutions for regulating and mitigating CO<sub>2</sub> emissions.

#### 4. Discussion and Conclusions

This paper addresses the temporal and spatial dynamics of CO<sub>2</sub> emissions from the water–atmosphere interface and their relationship with the meteorological and physico-chemical parameters of the water in three locations of wetlands (A, B, and C) formed along the Dambovita River, upstream from Lacul Morii lake, located in the peri-urban area of Bucharest, Romania. Using two closed chamber methods, the dynamic closed chamber EGM-5 method and the static closed chamber Injection Kit method, the provided values demonstrated the effectiveness of the EGM-5 method in detecting the more dynamic and fluctuating CO<sub>2</sub> emissions measured continuously in 5 min, while the Injection Kit proved to detect more static and discontinuous fluctuations in CO<sub>2</sub> emissions in 30 min.

Thus, the values obtained by the EGM-5 method proved to be higher than the Injection Kit method by 15% in the cold seasons and by approximately 32% higher in the warm seasons.

The statistical parameters for both methods, as Pearson correlation coefficients, were statistically significant in all three study locations, with  $r = 0.862$  ( $p < 0.01$ ) in location A,  $r = 0.812$  ( $p < 0.01$ ) in location B and  $r = 0.785$  ( $p < 0.01$ ) in location C, which validated the efficiency and complementarity of both methods in determining CO<sub>2</sub> emissions in aquatic ecosystems.

However, it is recommended to use the EGM-5 method as the basic method predominantly, and in the situations where the Injection Kit method is used, corrections are necessary based on temperature fluctuations associated with seasonal changes.

The extrapolation of the values measured in situ based on the relationships between  $T_{\text{air}}$ , pressure, and CO<sub>2</sub> emissions reveals distinct seasonal variability across the three locations. The integration of day–night variation ensures a high degree of confidence coefficients for these extrapolations, with values up to 76.88%, which provides consistency and reliability in the predictive models.

These findings align with the clear correspondence between CO<sub>2</sub> emissions from the water–atmosphere interface and temperature variations ( $T_{\text{air}}$  and  $T_{\text{water}}$ ). Significant positive correlations were identified in all three locations between CO<sub>2</sub> emissions measured by the EGM-5 method and  $T_{\text{air}}$  (correlation coefficients varying between 0.676 and 0.832; with statistical significance at the  $p < 0.01$  level), as well as with  $T_{\text{water}}$  (correlation coefficients varying between 0.677 and 0.793; with statistical significance at the  $p < 0.01$  level), while the Injection Kit method showed positive and statistically significant correlations varying between 0.598 and 0.777, with statistical significance at the  $p < 0.01$  level, respectively, and between 0.661 and 0.685, with statistical significance at the  $p < 0.01$  level. Regression analyses further reinforced these relationships, where the simple regression models demonstrated that  $T_{\text{air}}$  and pressure were significant predictors of CO<sub>2</sub> emissions across the three locations. The highest regression coefficients,  $R^2$  of 0.926 with the EGM-5 method and  $R^2$  of 0.933 with the Injection Kit method for  $T_{\text{air}}$ , and pressure regression values of  $R^2 = 0.989$  with EGM-5 and  $R^2 = 0.925$  with the Injection Kit method were observed in location B, indicating that temperature and pressure explained 92% of the variance in emissions, but with statistically significant regression coefficient values in the other locations as well. These results highlight the influence of temperature and pressure on the release of CO<sub>2</sub> from the water–atmosphere interface. This observation is consistent with global patterns observed in other aquatic systems, where temperatures have been identified as key drivers of CO<sub>2</sub> fluxes [42–44]. The influence of precipitation and wind speed was minimal and statistically insignificant.

The spatial dynamics of CO<sub>2</sub> emissions along the three locations revealed significant differences, such that location A, characterised by dense vegetation and a natural river course, presented the highest CO<sub>2</sub> emissions, especially in the summer months, with a peak in June of 36.240 g m<sup>2</sup> d<sup>−1</sup> with the EGM-5 method and of 21.808 with the Injection Kit method. These increased values in location A align with findings from studies in similar vegetated wetlands, where high primary productivity contributes to elevated CO<sub>2</sub> emissions during warmer months [45,46]. Location B, being considered the transition

zone with mixed vegetation and a built riverbed, presented lower emissions, with maxima observed in August of  $3473 \text{ g m}^{-2} \text{ d}^{-1}$  with the EGM-5 method and  $3.926$  with the Injection Kit method, but the seasonal variation was less pronounced in comparison with location A, due to hydrological dynamics. Location C, situated near the reservoir, had the lowest  $\text{CO}_2$  emissions in all seasons, with a peak in June of  $3468 \text{ g m}^{-2} \text{ d}^{-1}$  with the EGM-5 method and a peak in July of  $2.372$  with the Injection Kit method. Reduced biological activity and possible sedimentation effects due to reservoir water dynamics and hydrological processes could explain the lower emissions and more complex seasonal pattern at this location.

Our depicted results for  $\text{CO}_2$  emissions along the Dambovita River indicated similar spatial variations to urban rivers connected to lakes in the subtropical monsoon climate regions of China [47,48], where  $\text{CO}_2$  emissions increased upstream compared to downstream and in the receiving lakes. Temporal variations showed similar trends with  $\text{CO}_2$  emissions from a rainwater wetland created in southern Finland [49], as well as from rivers and canals in the Danube Delta [50], where the monthly average  $\text{CO}_2$  emissions at the water–atmosphere interface during the peak growing season, from June to September, exceeded those of the other months.

Water quality parameters such as pH, dissolved oxygen concentration (DO), chlorophyll, and redox potential (ORP) were found to be the main water quality parameters influencing the variability of  $\text{CO}_2$  emissions. Thus, higher levels of ORP and chlorophyll were associated with increased  $\text{CO}_2$  emissions, while pH showed a negative correlation in all three locations.

The methodology developed and validated includes procedures for assessing  $\text{CO}_2$  emissions in order to establish their correlation with observed local conditions (weather, landscape, vegetation, etc.) for a better application of the analytical method. The applied methodologies improve the accuracy of the national GHG inventory by employing high-tier techniques adapted to wetland ecosystems, reducing the uncertainties in national GHG emission inventories. The study provides local environmental management with a scientific basis for implementing optimal climate adaptation strategies by prioritising management practises that mitigate emissions and increase carbon sequestration. Moreover, the integration of predictive models based on meteorological data (temperature and pressure) considerably enhances this study, offering an effective instrument for the replicability of spatial (three locations) and temporal (monthly and seasonal) variations in  $\text{CO}_2$  emissions for other similar case studies.

Future perspectives of the research activities presented in the paper aim for the improvement and application of the methodology at the national level in different wetland areas (like Danube Delta).

**Supplementary Materials:** The following supporting information can be downloaded at <https://www.mdpi.com/article/10.3390/atmos15111345/s1>, Table S1: Monthly mean Temperature ( $^{\circ}\text{C}$ ) and Pressure (kPa) from daily recorded data. Table S2: Extrapolated mean  $\text{CO}_2$  emissions in each location, based on models derived from data obtained using EGM-5 and Injection Kit methods. Table S3: Pearson correlation and linear regression coefficient of EGM-5 and water quality parameters. Table S4: Pearson correlation and linear regression coefficient of Injection Kit and water quality parameters.

**Author Contributions:** Conceptualisation, G.D., N.E. and L.L.; methodology, G.D., N.E., L.L., M.M. and M.G.B.; validation, G.D., M.M. and C.I.C.M.; formal analysis, G.D., N.E. and L.L.; investigation, N.E., L.L. and M.G.B.; resources, G.D., M.M. and M.G.B.; data curation, G.D., M.M., C.I.C.M.; writing—original draft preparation, G.D., N.E., L.L. and M.M.; writing—review and editing, G.D., M.M. and C.I.C.M.; visualisation, N.E., L.L. and M.G.B.; supervision, G.D.; project administration, G.D.; funding acquisition, G.D., M.M. and M.G.B. All authors have read and agreed to the published version of the manuscript.

**Funding:** This research is supported by the Romanian Ministry of Research, Innovation and Digitization, project PN 23 31 04 01/2023.

**Institutional Review Board Statement:** Not applicable.



**Informed Consent Statement:** Not applicable.

**Data Availability Statement:** Data is contained within the article or Supplementary Material.

**Acknowledgments:** This work was carried out through the Nucleu Program (44N/2023) within the National Plan for Research, Development and Innovation 2022–2027, supported by the Romanian Ministry of Research, Innovation and Digitization, project PN 23 31 04 01/2023.

**Conflicts of Interest:** The authors declare no conflicts of interest.

## References

- Intergovernmental Panel on Climate Change (IPCC). *2019 Refinement to the 2006 IPCC Guidelines for National Greenhouse Gas Inventories*; Calvo Buendia, E., Tanabe, K., Kranjc, A., Baasansuren, J., Fukuda, M., Ngarize, S., Osako, R., Pyrozhenko, Y., Shermanau, P., Federici, S., Eds.; IPCC: Geneva, Switzerland, 2019.
- UNFCCC. Land Use, Land-Use Change and Forestry (LULUCF). Available online: <https://unfccc.int/> (accessed on 17 January 2024).
- Böttcher, H.; Reise, J. *The Climate Impact of Forest and Land Management in the EU and the Role of Current Reporting and Accounting Rules*; Öko Institut: Berlin, Germany, 2020.
- Petrescu, R.; Peters, G.; Janssens-Maenhout, G.; Ciaia, P.; Tubiello, F.; Grassi, G.; Nabuurs, G.; Leip, A.; Garcia, C.G.; Winiwarter, W.; et al. European Anthropogenic AFOLU Greenhouse Gas Emissions: A Review and Benchmark Data. *Earth Syst. Sci. Data* **2020**, *12*, 961–1001. [[CrossRef](#)]
- Smith, J.E. *A Model of Forest Floor Carbon Mass for United States Forest Types*; U.S. Department of Agriculture, Forest Service, Northeastern Research Station: Newtown Square, PA, USA, 2002; Volume 722, p. 37.
- Camarada, M.; Gurrieri, S.; Valenza, M. Effects of Soil Gas Permeability and Recirculation Flux on Soil CO<sub>2</sub> Flux Measurements Performed Using a Closed Dynamic Accumulation Chamber. *Chem. Geol.* **2010**, *265*, 387–393. [[CrossRef](#)]
- Ota, M.; Yamazawa, H. Forest Floor CO<sub>2</sub> Flux Estimated from Soil CO<sub>2</sub> and Radon Concentrations. *Atmos. Environ.* **2010**, *44*, 4529–4535. [[CrossRef](#)]
- Al Makky, A.; Alaswad, A.; Gibson, D.R.; Olabi, A.G. Renewable Energy Scenario and Environmental Aspects of Soil Emission Measurements. *Renew. Sustain. Energy Rev.* **2017**, *68*, 1157–1173. [[CrossRef](#)]
- Avtar, R.; Tsusaka, K.; Herath, S. Assessment of Forest Carbon Stocks for REDD+ Implementation in the Muyong Forest System of Ifugao, Philippines. *Environ. Monit. Assess.* **2020**, *192*, 85. [[CrossRef](#)]
- Finlay, P.; Stobbs, R. Reporting Emissions of Greenhouse Gases in Canada. *Environ. Monit. Assess.* **1994**, *31*, 61–66. [[CrossRef](#)]
- Birdsey, B.; Kolka, R.; Smith, M.L.; Ryan, M.G.; Hollinger, D.; Heath, L.S.; Hoover, C.M. Landscape Carbon Monitoring and Analysis at the Experimental Forest Network. In Proceedings of the 3rd Annual Conference on Carbon Sequestration, Alexandria, VA, USA, 3–6 May 2004.
- European Commission. Land Use, Land Use Change and Forestry Regulation no 841/2018 for 2021–2030. 2018. Available online: <https://ec.europa.eu/> (accessed on 18 July 2024).
- Romppanen, S. The LULUCF Regulation: The New Role of Land and Forests in the EU Climate and Policy Framework. *J. Energy Nat. Resour. Law* **2020**, *38*, 261–287. [[CrossRef](#)]
- Wulder, M.A.; White, J.C.; Stinson, G.; Hilker, T.; Kurz, A.W.; Coops, N.C.; St-Onge, B.; Trofymow, J.A. Implications of Differing Input Data Sources and Approaches Upon Forest Carbon Stock Estimation. *Environ. Monit. Assess.* **2010**, *166*, 543–561. [[CrossRef](#)]
- Renzas, J.M.; Marín-Spiotta, E. *A Primer on Methods for Measuring Soil Carbon*; Land Tenure Center, University of Wisconsin-Madison: Madison, WI, USA, 2012.
- Pumpanen, J.; Kolari, P.; Ilvesniemi, H.; Minkkinen, K.; Vesala, T.; Niinistö, S.; Lohila, A.; Larmola, T.; Morero, M.; Pihlatie, M.; et al. Comparison of Different Chamber Techniques for Measuring Soil CO<sub>2</sub> Efflux. *Agric. For. Meteorol.* **2004**, *123*, 159–176. [[CrossRef](#)]
- Maier, M.; Schack-Kirchner, H.; Hildebrand, E.; Schindler, D. Soil CO<sub>2</sub> Efflux vs. Soil Respiration: Implications for Flux Models. *Agric. For. Meteorol.* **2011**, *151*, 1723–1730. [[CrossRef](#)]
- Kuzyakov, Y.; William, R.; Horwath, M.D.; Blagodatskaya, E. Review and Synthesis of the Effects of Elevated Atmospheric CO<sub>2</sub> on Soil Processes: No Changes in Pools, but Increased Fluxes and Accelerated Cycles. *Soil Biol. Biochem.* **2019**, *128*, 66–78. [[CrossRef](#)]
- György, D.; Rotaru, A.; Enache, N.A.; Laslo, L.; Matei, M.; Boboc, M.; Bara, N. Carbon Dioxide Sampling and Analysis Technologies for Aquatic and Terrestrial Ecosystems. *ECS Trans.* **2022**, *107*, 6525–6540. [[CrossRef](#)]
- Jauhiainen, J.; Alm, J.; Bjarnadottir, B.; Callesen, I.; Christiansen, J.R.; Clarke, N.; Dalsgaard, L.; He, H.; Jordan, S.; Kazanavičiūtė, V.; et al. Reviews and Syntheses: Greenhouse Gas Exchange Data from Drained Organic Forest Soils—A Review of Current Approaches and Recommendations for Future Research. *Biogeosciences* **2019**, *16*, 4687–4703. [[CrossRef](#)]
- Enache, N.; Laslo, L.; Matei, M.; Cătuneanu, I.; György, D.; Izahar, T.N.T. Analysis of the Results from the Applied Technologies for Carbon Dioxide Sampling in Aquatic Ecosystems. *IOP Conf. Ser. Earth Environ. Sci.* **2023**, *1216*, 012006. [[CrossRef](#)]
- Immirzi, C.P.; Maltby, E.; Clymo, R.S. *The Global Status of Peatlands and Their Role in Carbon Cycling*; Friends of the Earth: London, UK, 1992.
- Dilustro, J.J.; Collins, B.; Duncan, L.; Crawford, C. Moisture and Soil Texture Effects on Soil CO<sub>2</sub> Efflux Components in Southeastern Mixed Pine Forests. *For. Ecol. Manag.* **2005**, *204*, 87–97. [[CrossRef](#)]

24. Lee, S.J.; Yim, J.S.; Son, Y.M.; Son, Y.; Kim, R. Estimation of Forest Carbon Stocks for National Greenhouse Gas Inventory Reporting in South Korea. *Forests* **2018**, *9*, 625. [[CrossRef](#)]
25. Davidson, E.A.; Janssens, I.A. Temperature Sensitivity of Soil Carbon Decomposition and Feedback to Climate Change. *Nature* **2006**, *440*, 165–173. [[CrossRef](#)]
26. Li, G.; Xiao, K.; Wang, Q.; Zhang, Y.; Li, H.; Li, H.; Shi, L. Forest Management and Carbon Sequestration of Larch Forests in China: A Review. *For. Ecol. Manag.* **2018**, *424*, 301–312.
27. György, D.; Enache, N.; Laslo, L.; Rotaru, A.; Matei, M.; Boboc, M.; Silaghi, C.; Calin, S.; Keresztesi, Á.; Kilar, F. CO<sub>2</sub> Efflux Measurements on Aquatic and Terrestrial Ecosystems in the Context of Climate Change. *Int. J. Conserv. Sci.* **2022**, *13*, 705–716.
28. Bridgham, S.D.; Cadillo-Quiroz, H.; Keller, J.K.; Zhuang, Q. Methane Emissions from Wetlands: Biogeochemical, Microbial, and Modelling Perspectives from Local to Global Scales. *Glob. Chang. Biol.* **2013**, *19*, 1325–1346. [[CrossRef](#)]
29. Enache, N.; Laslo, L.; György, D.; Matei, M.; Boboc, M.; Yusuf, S.Y. Seasonal Sensitivity of Reco from Aquatic Ecosystems to Meteorological and Physicochemical Water Parameters. *E3S Web Conf.* **2023**, *437*, 02012. [[CrossRef](#)]
30. Zhang, Z.; Liu, X.; Cai, Z.; Jiang, P.; Chen, J.; Chen, X. Effects of Meteorological Factors and Soil Properties on Soil CO<sub>2</sub> Flux from Wetlands of a Cold Temperate Forested Region, Northeastern China. *Ecol. Indic.* **2018**, *85*, 302–311.
31. Blue Marble Geographics. Global Mapper, v23. 2022. Available online: <https://www.bluemarblegeo.com> (accessed on 11 July 2024).
32. Meteoromania. Caracterizare Anuală. 2022. Available online: [https://www.meteoromania.ro/clim/caracterizare-anuala/cc\\_2022.html](https://www.meteoromania.ro/clim/caracterizare-anuala/cc_2022.html) (accessed on 27 June 2024).
33. PP Systems. EGM-5 Portable CO<sub>2</sub> Gas Analyzer. Available online: <https://ppsystems.com/egm-5/> (accessed on 27 June 2024).
34. Garnett, M.H.; Newton, J.-A.; Parker, T.C. A Highly Portable and Inexpensive Field Sampling Kit for Radiocarbon Analysis of Carbon Dioxide. *Radiocarbon* **2021**, *63*, 1355–1368. [[CrossRef](#)]
35. Laslo, L.; Matei, M.; Boboc, M.; György, D.; Cătuneanu, I.; Enache, N.; Nurliza, R. Measurements and Statistical Analysis of CO<sub>2</sub> Efflux and Related Parameters from Crop and Forested Lands. *IOP Conf. Ser. Earth Environ. Sci.* **2023**, *1216*, 012005. [[CrossRef](#)]
36. NASA Power. NASA power Data Access Viewer. Available online: <https://power.larc.nasa.gov> (accessed on 14 August 2024).
37. Voicu, M.; Coman, V.; Enache, N.; Laslo, L.; Matei, M.; Rotaru, A.; Bara, N.; Boboc, M.; Stanciu, S.; György, D. Experimental Determination of Carbon Dioxide Flux in Soil and Correlation with Dependent Parameters. *IOP Conf. Ser. Earth Environ. Sci.* **2020**, *616*, 012010. [[CrossRef](#)]
38. Yin, X.; Jiang, C.; Xu, S.; Yu, X.; Yin, X.; Wang, J.; Maihaiti, M.; Wang, C.; Zheng, X.; Zhuang, X. Greenhouse Gases Emissions of Constructed Wetlands: Mechanisms and Affecting Factors. *Water* **2023**, *15*, 2871. [[CrossRef](#)]
39. Mondal, B.; Bauddh, K.; Kumar, A.; Bordoloi, N. India's Contribution to Greenhouse Gas Emission from Freshwater Ecosystems: A Comprehensive Review. *Water* **2022**, *14*, 2965. [[CrossRef](#)]
40. Han, X.; Shi, W.-Y.; Yao, Y.-X. A Review of the Water–Carbon Nexus in Urban Systems. *Water* **2023**, *15*, 1005. [[CrossRef](#)]
41. Cohen, J. *Statistical Power Analysis for the Behavioural Sciences*, 2nd ed.; Lawrence Erlbaum Associates: Hillsdale, NJ, USA, 1988.
42. Salimi, S.; Almutkar, A.; Scholz, M. Impact of climate change on wetland ecosystems: A critical review of experimental wetlands. *J. Exp. Med.* **2021**, *286*, 112160. [[CrossRef](#)]
43. Shuzhen, L.; Jialiang, Z.; Qiang, L.; Liqiao, L.; Tao, S.; Xiaofeng, X.; Miao, L.; Xuan, W.; Xiaomin, Y. Warming influences CO<sub>2</sub> emissions from China's coastal saltmarsh wetlands more than changes in precipitation. *Sci. Total Environ.* **2023**, *881*, 163551. [[CrossRef](#)]
44. Pinho, L.; Duarte, C.M.; Marotta, H.; Enrich-Prast, A. Temperature dependence of the relationship between pCO<sub>2</sub> and dissolved organic carbon in lakes. *Biogeosciences* **2016**, *13*, 865–871. [[CrossRef](#)]
45. Miller, R.L.; Fujii, R. Plant community, primary productivity, and environmental conditions following wetland re-establishment in the Sacramento-San Joaquin Delta, California. *Wetl. Ecol Manag.* **2010**, *18*, 1–16. [[CrossRef](#)]
46. Kang, X.; Hao, Y.; Cui, X.; Chen, H.; Huang, S.; Du, Y.; Li, W.; Kardol, P.; Xiao, X.; Cui, L. Variability and Changes in Climate, Phenology, and Gross Primary Production of an Alpine Wetland Ecosystem. *Remote Sens.* **2016**, *8*, 391. [[CrossRef](#)]
47. Liu, B.; Zhang, R.; Zhu, L.; Wang, J.; Qin, B.; Shi, W. An outsized contribution of rivers to carbon emissions from interconnected urban river-lake networks within plains. *Geophys. Res. Lett.* **2024**, *51*, e2023GL107250. [[CrossRef](#)]
48. Wang, C.; Xv, Y.; Li, S.; Li, X. Interconnected River–Lake Project Decreased CO<sub>2</sub> and CH<sub>4</sub> Emission from Urban Rivers. *Water* **2023**, *15*, 1986. [[CrossRef](#)]
49. Li, X.; Wahlroos, O.; Haapanala, S.; Pumpanen, J.; Vasander, H.; Ojala, A.; Vesala, T.; Mammarella, I. Carbon dioxide and methane fluxes from different surface types in a created urban wetland. *Biogeosciences* **2020**, *17*, 3409–3425. [[CrossRef](#)]
50. Maier, M.-S.; Teodoru, C.R.; Wehrli, B. Spatio-temporal variations in lateral and atmospheric carbon fluxes from the Danube Delta. *Biogeosciences* **2021**, *18*, 1417–1437. [[CrossRef](#)]

**Disclaimer/Publisher's Note:** The statements, opinions and data contained in all publications are solely those of the individual author(s) and contributor(s) and not of MDPI and/or the editor(s). MDPI and/or the editor(s) disclaim responsibility for any injury to people or property resulting from any ideas, methods, instructions or products referred to in the content.